



THE UNIVERSITY *of* EDINBURGH

Edinburgh Research Explorer

Numerical Investigation on the Progressive Collapse Behavior of Precast Reinforced Concrete Frame Sub-assemblages

Citation for published version:

Feng, D-C, Wu, G & Lu, Y 2018, 'Numerical Investigation on the Progressive Collapse Behavior of Precast Reinforced Concrete Frame Sub-assemblages', *Journal of Performance of Constructed Facilities*, vol. 32, no. 3, 04018027, pp. 1-14.

Link:

[Link to publication record in Edinburgh Research Explorer](#)

Document Version:

Peer reviewed version

Published In:

Journal of Performance of Constructed Facilities

General rights

Copyright for the publications made accessible via the Edinburgh Research Explorer is retained by the author(s) and / or other copyright owners and it is a condition of accessing these publications that users recognise and abide by the legal requirements associated with these rights.

Take down policy

The University of Edinburgh has made every reasonable effort to ensure that Edinburgh Research Explorer content complies with UK legislation. If you believe that the public display of this file breaches copyright please contact openaccess@ed.ac.uk providing details, and we will remove access to the work immediately and investigate your claim.



Numerical Investigation on the Progressive Collapse Behavior of Precast Reinforced Concrete Frame Sub-assemblages

De-Cheng Feng¹, Gang Wu², and Yong Lu³

¹Key Laboratory of Concrete and Prestressed Concrete Structures of the Ministry of Education, Southeast University, 2 Sipailou, Nanjing 210096, China

²Key Laboratory of Concrete and Prestressed Concrete Structures of the Ministry of Education, Southeast University, 2 Sipailou, Nanjing 210096, China, with corresponding author. Email: g.wu@seu.edu.cn

³Institute for Infrastructure and Environment, School of Engineering, The University of Edinburgh, Edinburgh EH9 3JL, UK

ABSTRACT

This paper presents a numerical investigation of the progressive collapse behavior of the precast reinforced concrete (RC) frame sub-assemblages. An efficient numerical model for the precast RC frame sub-assemblages under progressive collapse is developed based on OpenSEES software, where the fiber beam element is used for the beams and columns and the Joint2D element is used for the beam-to-column connections. To consider the significant bond-slip effect inside the joint core of the precast RC frame sub-assemblages, the stress-slip relationship for reinforcement bars with different embedded lengths is derived and used to generate the force-deformation relation for the springs incorporated in the Joint2D element. The numerical model is validated through comparisons with the experimental results of RC sub-assemblages subjected to column removal scenarios in terms of load-displacement curve, compressive arch action, catenary action capacity, etc. Finally systematic parametric studies are conducted based on the validated numerical model to investigate the influences of some typical parameters that involved in precast RC structures on the progressive collapse capacity of the sub-assemblages.

25 **Keywords:** progressive collapse, precast, RC frame sub-assemblages, numerical simulation,
26 OpenSEES

27 INTRODUCTION

28 Progressive collapse of reinforced concrete (RC) structures has caught widespread attentions
29 around the world in recent years, since great loss of public properties and human lives has been
30 caused by progressive collapse of structures, and there has been an increasing trend of extreme
31 events due to malicious attacks, accidental gas explosion and vehicle impact, etc.([Ellingwood](#)
32 [2006](#)). To mitigate the progressive collapse risk of RC structures, some specific methods have been
33 developed in various design codes and guidelines, e.g., General Service Administration (GSA)
34 2013 ([GSA 2013](#)) and Department of Defense (DoD) 2013 ([DoD 2013](#)). Among the proposed
35 design methods, the alternate load path (ALP) method is the most commonly used one due to its
36 efficiency and ease of operation ([Pham et al. 2016](#)). With this method, one middle column will be
37 removed to check whether the remaining structure can bridge over the missing column. Although
38 simply removing one column in the ALP method does not simulate the real initial damage scenario
39 (a complete removal of a column is rarely seen in real incidents), it is considered as an effective
40 way to assess the progressive collapse potential.

41 In light of the fundamental concepts of ALP approach, several experimental tests of RC beam-
42 column sub-assemblages subjected to column removal scenarios have been conducted in the litera-
43 ture to investigate their progressive collapse resistance, i.e., the work done by Sasani and Kropelnicki
44 ([Sasani and Kropelnicki 2008](#)), Yi et al. ([Yi et al. 2008](#)), Su et al. ([Su et al. 2009](#)), Yap and Li
45 ([Yap and Li 2011](#)), Qian and Li ([Qian and Li 2012](#)), Yu and Tan ([Yu and Tan 2013](#)), Ren et al.
46 ([Ren et al. 2016](#)), Lu et al. ([Lu et al. 2016](#)) and Qian et al. ([Qian et al. 2016](#)), etc. However,
47 although experimental studies can provide first-hand results of RC frame sub-assemblages against
48 progressive collapse, conducting such experiments are generally very costly and time consuming.
49 Furthermore, due to the constraints of the experimental facilities and space, among other factors,
50 it is impractical to investigate the influence of a variety of parameters on the progressive collapse
51 behavior using physical experiments.

52 On the other hand, many numerical models have also been developed to study the progressive
53 collapse behavior of RC frame sub-assemblages. Generally, the models may be grouped into
54 three categories: the detailed finite element models, the fiber element-based models and the macro
55 component-based models. Detailed finite element models (Sasani et al. 2011; Qian and Li 2011;
56 Bao et al. 2012; Pham et al. 2016) usually adopt three-dimensional (3D) solid elements to simulate
57 the behavior of an RC sub-assemblage, and the detailed local responses including concrete cracking
58 and crushing, steel yielding and fracture, can be obtained. However, the computational effort of
59 this approach is extremely demanding and oftentimes some convergence issues may also arise.
60 Fiber element-based models (Valipour and Foster 2010; Li et al. 2011; Brunesi and Nascimbene
61 2014; Brunesi et al. 2015; Feng et al. 2016a; Yu et al. 2016; Brunesi and Parisi 2017) use fiber
62 beam-column elements with co-rotational formulation to model the structure, in which the large
63 deformation effect is well considered. This approach is much faster than using detailed finite
64 element models, and the numerical accuracy in terms of the global response can also be guaranteed
65 (Li et al. 2016a; Li et al. 2016b). However, some specific failure modes, e.g, bond-slip and bar
66 fracture, cannot be reflected. The macro component-based models (Bao et al. 2008; Yu and Tan
67 2014) strive to achieve an adequate balance between the analysis accuracy and computational
68 efficiency. In this type of models, fiber elements are still used to model beams and columns, but
69 additional component-based joint model consisting of series of springs is introduced to represent
70 the essential mechanisms of a beam-to-column connection; thus local failure in the joint region such
71 as the bar slip and fracture can be incorporated. For these reasons, the macro component-based
72 models are deemed more suitable for the progressive collapse analysis of RC frame assemblages.

73 So far the existing studies, either experimental or numerical, have mainly focused on the
74 monolithic RC structures, while little attention has been paid on the progressive collapse capacity
75 of precast RC structures. Actually, the precast structures are now widely used around the world
76 due to various advantages such as the product quality, construction speed, and so on. Especially in
77 rapidly developing countries like China, there is a great demand for precast structures due to the
78 rapid process of urbanization. Therefore, there is an urgent need to study the progressive collapse

79 behavior of precast structures. Kang and Tan (Kang and Tan 2015a; Kang and Tan 2017) conducted
80 a set of experiments to investigate the progressive collapse capacity of precast sub-assemblages, and
81 some special features that are unique in precast structures, e.g., discontinuous reinforcement, were
82 also analyzed. However, no numerical model has been developed for precast RC sub-assemblages
83 under a progressive collapse scenario up till now. Compared with the monolithic RC structures, the
84 bond-slip effect is particularly significant in precast structures since the post-cast concrete quality
85 can hardly be guaranteed (Kang and Tan 2015b), and therefore careful handling of this important
86 feature is required in a numerical model.

87 Based on the above-mentioned aspects, this paper aims at developing an efficient numerical
88 model for precast RC frame sub-assemblages against progressive collapse based on the software
89 OpenSEES, and subsequently performing systemic parametric studies to investigate the progressive
90 collapse behavior of precast sub-assemblages. First the numerical model is introduced in detail,
91 where the fiber beam element is used for the beams and columns and the Joint2D element is used
92 for the beam-to-column connections. In particular, an analytical stress-slip model is derived for
93 the beam reinforcement in the middle joint of a precast sub-assemblage. The developed numerical
94 model is then validated through comparison with the experimental results of the precast sub-
95 assemblages under a column removal scenario. With the validated numerical model, systematic
96 parametric studies are conducted to study the influences of some unique parameters in precast RC
97 structures on its progressive collapse performance.

98 **PROGRESSIVE COLLAPSE MODELING APPROACH BASED ON OPENSEES**

99 As mentioned before, the progressive collapse process of precast frame sub-assemblages in-
100 volves several complex behavioral developments of the structure, including material nonlinearity,
101 geometrical nonlinearity, bond-slip effect, and bar fracture. Furthermore, the force transfer mecha-
102 nism from beams to columns through the connection part should also be clearly represented in the
103 numerical model. Although a detailed model involving continuum solid elements can capture these
104 local responses, the numerical efficiency and convergence issue remain a problem. Therefore, an
105 alternative marco-level element approach based on fiber element and Joint2D element (Altoontash

106 2004), which are available in OpenSEES, is adopted in this paper to simulate the progressive
107 collapse behavior of precast sub-assemblages.

108 **Proposed modeling approach for precast sub-assemblage**

109 In the proposed numerical modeling of the precast sub-assemblages, conventional displacement-
110 based (DB) fiber beam-column elements are used to simulate the beams and columns, while Joint2D
111 element is used to model the beam-to-column connection, as indicated in Fig. 1. The fiber element
112 is based on co-rotational formulation to include large deformation effect, and Gauss-Legendre
113 quadrature is used in the element. The cross-section of the element is divided into concrete and
114 reinforcement fibers, and each fiber has its own uniaxial constitutive law. Different fibers can have
115 different constitutive laws, and thus the properties of precast and post-cast concrete can be assigned
116 separately and the confinement effect provided by stirrups can also be considered. The concrete
117 damage-plasticity model (ConcreteD), which is implemented in OpenSEES and recommended in a
118 Chinese code for design of concrete structures (Ministry of Construction of the People's Republic of
119 China 2010), and the bilinear steel model (Steel01) are adopted for concrete and reinforcement
120 fibers, respectively. The details for the two material models are given in Appendix I and II.

121 The Joint2D element is developed by Altoontash (Altoontash 2004), which is actually a sim-
122 plified version of the BeamColumnJoint element in OpenSEES (Lowe and Altoontash 2003), and
123 large deformation effect can also be accounted for in the model. Although similar component-based
124 joint models are also proposed in the literature (Bao et al. 2008; Yu and Tan 2013; Yu and Tan 2014)
125 to model the progressive collapse behavior of RC sub-assemblages, they seem to be more com-
126 plicated and need complex calibration of the component properties. The proposed element herein
127 modifies the original Joint2D element to suit for a progressive collapse analysis, and consists of five
128 spring components, representing the shear distortion of the joint panel and the moment-rotation
129 behavior including the bar bond-slip effect of the section at the four ends of beams and columns,
130 respectively. The five spring components are defined with uniaxial force-deformation relations
131 (Altoontash 2004). For the central shear spring, usually the shear stress-strain relation $\tau - \gamma$ is
132 determined based on the modified compression field theory (MCFT) (Vecchio and Collins 1986)

133 or the softened truss model (STM) (Hsu 1988), and then it is converted to the equivalent moment-
134 rotation relation $M - \theta$ of the joint panel with the following expressions: $M = \tau V_J$, $\theta = \arctan \gamma$,
135 where V_J is the volume of the panel. However, several studies indicate that there is no significant
136 shear deformation of the joint panel when the sub-assembly is under progressive collapse, since
137 the joint is subjected to vertical displacement and restrained by the surrounding beam and columns
138 (Bao et al. 2008; Yu and Tan 2013; Yu and Tan 2014; Rashidian et al. 2016). Hence, the shear
139 spring is assumed to be elastic in this paper, enabling a rigid shear panel behavior. For the interface
140 springs at the beam and column ends, which actually represents the member-end rotation due to
141 bond-slip effect, the corresponding force-deformation relation is calibrated based on a fiber section
142 analysis (unit length) with the stress-strain relation for the steel fibers replaced by the stress-slip
143 relation (Altoontash 2004), and the bar fracture is considered through a Min-Max criterion material
144 in OpenSEES (Feng et al. 2016a). Moreover, the column end springs can be further simplified
145 as rigid since no failure would occur at the column-joint interface when the sub-assembly is
146 under a column removal scenario. The stress-slip relation of the steel fibers can be obtained from
147 either experimental results or theoretical derivation, and the generated section force-deformation
148 relationship is then simplified into a tri-linear relationship by getting the critical points and assigned
149 to the springs, which can be done by the Hysteretic material model in OpenSEES, as shown in
150 Fig. 2. A summary of the proposed modeling approach is given in Table 1.

151 It should be noted that in modelling the joint it is usually assumed that the rebar development
152 length is sufficient (Altoontash 2004); however, this may be not true for precast structure, especially
153 for the bottom reinforcement of the beam under a column removal scenario. Therefore, a stress-slip
154 model for the reinforcement bars of the beam with different embedded lengths is derived in the next
155 section to address this situation.

156 **Analytical derivation of the stress-slip behavior of reinforcement**

157 The bond-slip effect is an important factor that influences the progressive collapse behavior of the
158 precast sub-assembly, since the reinforcement may develop large strain under a column removal
159 scenario and thereby bond failure could occur. Especially, this effect is even more significant

for precast structures since the quality of the post-cast concrete in the joint core region cannot be guaranteed as the monolithic structures. Moreover, although some of the existing macro-models can account for bond-slip effect, there is commonly an associated assumption that the embedded length for bars is sufficient; consequently the applicability is restricted, especially for precast concrete structures.

In the present modeling approach introduced in the previous subsection, the bond-slip effect is considered through the beam interface springs in the Joint2D element, and the spring properties are calibrated through a unit length fiber section analysis discussed before. Hence, a stress-slip model is needed herein.

The bond-slip behavior of the beam reinforcement when subjected to progressive collapse actually depends on the anchorage type. Generally, three kinds of anchorage are used in precast RC structures, namely, continuous, lap-spliced and hooked, as shown in Fig. 3. The total slip s of the reinforcement is actually given by the integral of the strain distribution $\epsilon(x)$ along the embedded length L_{embed} , i.e.,

$$s = \int_0^{L_{embed}} \epsilon(x) dx \quad (1)$$

Assuming that the bond stress is a stepped distribution (Sezen and Setzler 2008), as shown in Fig. 3, the total slip of the reinforcement can be analytically derived based on the static equilibrium condition and Eq. (1). Denoting the strain at the loaded end as ϵ_s and the yielding strain as ϵ_y , the bond stress for elastic part ($\epsilon_s \leq \epsilon_y$) and plastic part ($\epsilon_s > \epsilon_y$) are defined as $u_{be} = 1.8\sqrt{f'_c}$ and $u_{by} = 0.5\sqrt{f'_c}$, respectively, where f'_c is the cubic compressive strength of concrete (Yu and Tan 2014). The detailed slip derivation for different anchorage types are given as follows:

* *For continuous bar* (Fig. 3(a))

When a precast sub-assembly is subjected to progressive collapse in a typical middle column removal scenario, the continuous reinforcement inside the joint will finally stress up to the center of the joint under catenary action, and the embedded length of the reinforcement actually equals half of the column width h_c , i.e., $L_{embed} = 0.5h_c$. The development of the slip

can be divided into three stages. At first the bar is elastic and the corresponding developed elastic bond length L_{ed} can be determined by the force equilibrium

$$L_{ed} = \frac{f_s d_b}{4u_{be}} \quad (2)$$

where d_b is the bar diameter; f_s is the reinforcement stress. Then the slip is obtained through Eq. (1)

$$s = \int_0^{L_{ed}} \epsilon(x) dx = \frac{\epsilon_s}{2} L_{ed} \quad (3)$$

After that the bar yields but is not stressed up to the center, the yielded length L_{yd} is given by

$$L_{yd} = \frac{(f_s - f_y) d_b}{4u_{by}} \quad (4)$$

and the slip is computed as

$$s = \int_0^{L_{ed}} \epsilon(x) dx + \int_{L_{ed}}^{L_{yd}} \epsilon(x) dx = \frac{\epsilon_y}{2} L_{ed} + \frac{\epsilon_y + \epsilon_s}{2} L_{yd} \quad (5)$$

Finally, the reinforcement is stressed up to the center of the joint under catenary action, but the slip at the center point is still zero due to symmetry. The corresponding elastic developed length and yielded developed length are

$$L_{yd} = \frac{(f_s - f_y) d_b}{4u_{by}}, \quad L_{ed} = L_{embd} - L_{yd} \quad (6)$$

and the slip is

$$s = \int_0^{L_{ed}} \epsilon(x) dx + \int_{L_{ed}}^{L_{yd}} \epsilon(x) dx = \frac{\epsilon_{end} + \epsilon_y}{2} L_{ed} + \frac{\epsilon_y + \epsilon_s}{2} L_{yd} \quad (7)$$

where ϵ_{end} can be determined through similar triangle method. Note that no pull-out failure will occur in this case.

205

206

* For lap-spliced and hooked bar (Fig. 3(b) and 3(c))

207

208

209

210

211

212

Unlike the case with continuous bar, the bond stress of lap-spliced and hooked bar may develop until to the free-end; the strain and stress at the free-end should be zero and the strain profile should be modified to the blue dashed line in Fig. 4. The free-end slip (if any) should be also included in the total slip. The embedded length for lap-spliced bar is the realistic one, while for hooked bar, it can be modelled as a straight bar with an equivalent length of (Yu and Tan 2014)

213

$$L_{embd} = L_{embd}^s + 5d_b \quad (8)$$

214

where L_{embd}^s is the straight embedment length of the hooked bar.

215

216

According to the relation between the embedded length and developed bond length and the assumption discussed above, as shown in Fig. 4, the slip is derived as follows:

217

218

219

220

• If the bar embedded length is sufficient to develop full bond length L_d (Fig. 4(a)), the failure mode is bar fracture, the developed process of the bond stress involves two stages. At first the bar is elastic, and developed elastic bond length L_{ed} and corresponding slip are given by

221

$$L_{ed} = \frac{f_s d_b}{4u_{be}}, \quad s = \int_0^{L_{ed}} \epsilon(x) dx = \frac{\epsilon_s}{2} L_{ed} \quad (9)$$

222

Then the bar yields, and the yield length and slip are

223

$$L_{yd} = \frac{(f_s - f_y) d_b}{4u_{by}}, \quad s = \int_0^{L_{ed}} \epsilon(x) dx + \int_{L_{ed}}^{L_{yd}} \epsilon(x) dx = \frac{\epsilon_y}{2} L_{ed} + \frac{\epsilon_y + \epsilon_s}{2} L_{yd} \quad (10)$$

224

225

226

227

• If the bar embedded length is sufficient to develop elastic bond length but not sufficient to develop full bond length (Fig. 4(b)), the first two stages of slip evolution are the same with Eqs. (9) and (10) in last case. However, the bar will be stressed up to the free-end, and free

end slip may occur. So the developed length and slip in this situation are expressed as

$$L_{yd} = \frac{(f_s - f_y) d_b}{4u_{by}}, \quad L_{ed} = L_{embd} - L_{yd} \quad (11)$$

$$s = s_0 + \int_0^{L_{ed}} \epsilon(x) dx + \int_{L_{ed}}^{L_{yd}} \epsilon(x) dx = s_0 + \frac{\epsilon_y}{2} L_{ed} + \frac{\epsilon_y + \epsilon_s}{2} L_{yd} \quad (12)$$

where s_0 is the free-end slip and can be determined by

$$s_0 = s_1 \left(\frac{u_e}{u_u} \right)^{2.5} \quad (13)$$

with

$$s_1 = \left(\frac{30}{f'_c} \right)^{0.5}, \quad u_e = \frac{f_{se} d_b}{4L_{edb}}, \quad u_u = \left(20 - \frac{d_b}{4} \right) \left(\frac{f'_c}{30} \right)^{0.5} \quad (14)$$

where s_1 is the ultimate slip at the free-end; u_e is the elastic bond stress at the free-end; u_u is the ultimate bond stress; f_{se} is the maximum bar stress ($\leq f_y$) in the elastic developed bond length. Note that if u_e reaches u_u ($s_0 \geq s_1$), the bar will fail by a pull-out mode.

- If the bar embedded length is even not sufficient to develop elastic bond length (Fig. 4(c)), at first it is still the same as Eq. (9), then the bar will be stressed up when the applied strain is even in the elastic stage; the developed elastic bond length is actually the full embedded length, i.e., $L_{ed} = L_{embd}$, thus the slip is

$$s = s_0 + \int_0^{L_{ed}} \epsilon(x) dx = s_0 + \frac{\epsilon_s}{2} L_{embd} \quad (15)$$

If there is no pull-out failure ($s_0 \geq s_1$) even when the bar yields at the loaded end, then the slip is the same as Eq. (12).

With the above equations, the reinforcement stress-slip relation can be obtained. Note that two kinds of bar failure modes may happen, namely, fracture failure ($\epsilon_s \geq \epsilon_u$) and pull-out failure

249 ($s_0 \geq s_1$); here whichever mode is first reached will be treated as the failure of the bar. Meanwhile,
250 the bond-slip effect is neglected for reinforcement under compression in this paper. In fact, when
251 subjected to progressive collapse, the reinforcement will eventually undergo tension to develop
252 catenary action, thus the bond-slip behavior under compression will have little influence on its
253 global performance.

254 **Nonlinear solution strategy**

255 The numerical simulation of progressive collapse of precast sub-assembly includes several
256 extreme behaviors, i.e., material and geometrical nonlinearity, bar fracture etc. Therefore, some
257 convergence issue may arise in the simulation and the numerical solution algorithm is a challenge
258 aspect. To improve the numerical performance, a varying solution strategy is employed in this paper.
259 The analysis starts with the full Newton-Raphson algorithm, which has the fastest convergence rate,
260 and the convergence tolerance is set as 10^{-6} on the norm of energy increment. The maximum
261 number of iterations for each time step is defined as 200. If the solution cannot be obtained in a
262 single step, the analysis switches the algorithm in turn to modified Newton-Raphson method, Krylov
263 Newton acceleration method and Newton line search method until the convergence is attained. If it
264 still fails to obtain a solution, the iteration number is increased (i.e., 1000). If a solution still cannot
265 be obtained, a larger tolerance is then adopted (i.e., 10^{-4}). After the convergence is obtained, all
266 these settings are returned back to the default ones for the next step.

267 **VALIDATION OF THE PROPOSED MODELING APPROACH**

268 **Overview of progressive collapse test on precast RC sub-assemblages**

269 To validate the proposed numerical modeling approach for precast RC sub-assemblages, the
270 experiments conducted by Kang and Tan's group ([Kang and Tan 2015a](#); [Kang et al. 2015](#)) are
271 simulated. The experiments were performed to investigate whether the precast sub-assemblages
272 could develop catenary action under column removal, even though they could exhibit similar
273 seismic performance as the monolithic structures. Totally six specimens, designed in accordance
274 with Eurocode 2, were tested. The geometrical dimensions were kept the same, and the differences

275 came from the reinforcing details. Each specimen was made up of two precast beam units and two
276 end column stubs, and the precast components were assembled in the joint region through cast-
277 in-situ concrete. The span for the beams was 2750 mm, while the cross-section dimensions were
278 300×150 mm for beams, 250×250 mm for middle columns and 400×450 mm for end column
279 stubs. Two kinds of reinforcing details were used in the connection region, namely, hooked (90°
280 bent) and lap-spliced, as shown in Fig. 5. Apart from the reinforcing details, the main investigating
281 parameter was the reinforcing ratio, which is listed in Table 2.

282 The material properties of the specimens, including concrete and reinforcement, are given in
283 Table 3, where bar H13 and H16 marked with * were used for specimen MJ-B-1.19/0.59R only.
284 The two end column stubs were restrained each by two load cells in in the horizontal direction,
285 and one pin support in the vertical direction. In addition, two sets of steel columns were arranged
286 on each side of the middle span of the beams to prevent out-of-plane failure of the specimens.
287 Column removal was simulated through gradually increasing the vertical displacement at the top
288 of the middle column stub. More details about the experiments can be found in (Kang and Tan
289 2015a; Kang et al. 2015).

290 **Analysis results**

291 The established numerical model is demonstrated in Fig. 6. The beams and columns are modeled
292 with fiber elements, and the joints are represented with the Joint2D model discussed above. The
293 finite element mesh size is defined as the section height to avoid softening localization issue (Feng
294 et al. 2015), and two integration points are used for each element. The sections are divided into
295 two parts, i.e., the precast part and the cast-in-situ part, and each part is discretized into 20 concrete
296 fibers, and the number and locations of the steel fibers are assigned according to the reinforcement
297 detail of each beam and column. Material model parameters are determined according to Table 2,
298 and the concrete tensile strength is given by $0.25\sqrt{f_c}$, where f_c is the compressive strength. The
299 confinement effect is considered through Mander model (Mander et al. 1988). The embedded
300 length for the continuous reinforcement bars is set as half of the column width, i.e., 125 mm, and
301 for the bent bar it is $190 + 5d_b$ mm and for the lap-spliced bar it is 470 mm. The boundary conditions

302 of the end column stubs are simulated with lateral elastic springs, and the stiffness is assumed to be
303 the level of 10^5 kN/m, which is consistent with the recommendation in (Yu and Tan 2013) based on
304 the measurement of the reaction forces and the displacements. Vertical load is applied at the top of
305 the middle column stub through displacement control, and for a quasi static analysis the time step
306 is set as 1 mm/s.

307 The simulated vertical displacement of the middle column versus the vertical applied load on the
308 column top, as well as the horizontal reaction forces of the beams (or the beam axial forces) of all the
309 six specimens are plotted against the experimental results in Fig. 7. Good agreements are achieved
310 between the numerical and experimental results for nearly all the specimens. It can be found from
311 the applied load-vertical displacement curves that the initial stiffness, flexural beam action, and
312 the effects of compressive arch action (CAA) and catenary action all can be well reflected by the
313 numerical model. Furthermore, the bar fracture failure at the middle column joint and end column
314 stubs can also be reproduced.

315 More specifically, the CAA capacities predicted by the numerical model for specimens MJ-
316 B-0.52/0.35S, MJ-B-0.88/0.59R, MJ-B-1.19/0.59R and MJ-L-0.52/0.35S are nearly the same as
317 the experimental results, while they are 6 kN and 8.3 kN larger than the experimental values for
318 specimens MJ-L-0.88/0.59R and MJ-L-1.19/0.59R, respectively, which corresponds to the relative
319 differences of 11% and 14% between the numerical and experimental results. The numerical
320 models also predict quite well the bar fracture at the middle and end column joints for specimens
321 MJ-B-0.52/0.35S, MJ-B-1.19/0.59R and MJ-L-0.52/0.35S and MJ-L-1.19/0.59R, while the results
322 for specimens MJ-B-0.88/0.59R and MJ-L-0.88/0.59R are less comparable with the experimental
323 ones. This may be caused by the uncertainty in material properties, especially the fracture strain of
324 the reinforcement bars.

325 For the horizontal reaction force curves, the numerical results also exhibit good agreement with
326 the experimental results. Take the specimen MJ-B-0.88/0.59R as an example, the beam axial force
327 is first under compression and then transits to tension due to catenary action from a displacement
328 around 350 mm. The calculated maximum compression force is 282.7 kN which matches almost

329 exactly the measured value of 282.5 kN. Fig. 8 also gives the comparison of the deformed profile
330 of specimen MJ-B-0.88/0.59R under different vertical displacements obtained from the numerical
331 model and the experiment. As can be seen in the figure, the two sets of results match well with
332 each other. In general, the numerical results indicate that the developed finite element model can
333 predict realistically the responses of precast RC frame sub-assemblages, and therefore can be used
334 as an effective tool in a progressive collapse analysis.

335 **PARAMETRIC STUDIES ON PROGRESSIVE COLLAPSE BEHAVIOR OF PRECAST RC** 336 **SUB-ASSEMBLAGES**

337 With the validated numerical model, parametric studies can be performed to investigate the
338 influences of a variety of factors on the progressive collapse behavior of the precast RC sub-
339 assemblages. It is worth noting at this juncture that many basic design parameters, including
340 reinforcement ratio, beam depth, concrete strength, slab effect, boundary condition, etc., have been
341 widely studied before (Yu and Tan 2013; Yu and Tan 2014; Pham et al. 2016). The present study
342 therefore mainly focuses on a few factors that are particularly important for the analysis of precast
343 RC structures, namely, the modeling strategies, the strength of the cast-in-situ concrete, and the
344 anchorage length of the reinforcement bars at the joint region. To concentrate the observation
345 to these factors, the specimen MJ-L-0.88/0.59R is selected as a reference case to conduct the
346 parametric studies as described in the following subsections.

347 **Effect of modeling strategies**

348 First the effect of modeling strategies is discussed. The modeling strategy with elastic shear
349 spring as used in the above validation analysis is denoted as Model 1. To study the influence of
350 shear deformation at the joint region, Model 2 adopts a nonlinear shear spring property, which can
351 be obtained from MCFT. Model 3 employs a rigid joint model to investigate the influence of the
352 bond-slip effect, which means beam interface springs in the Joint2D model are set as rigid and the
353 bond-slip effect is neglected. Model 4 removes the Joint2D element and uses fiber element only
354 to simulate the sub-assemblages to improve the computational efficiency. However, to consider the
355 bond-slip effect, the stress-strain relationship of reinforcement in the critical nonlinear region is

356 modified by assuming that the equivalent strain is the sum of the slip and the bar deformation (Bao
357 et al. 2012), i.e., $\epsilon' = \epsilon + s/L_p$, where s is the bar slip derived above and L_p is the critical nonlinear
358 region length, usually equals beam height.

359 The results for the four models are demonstrated in Fig. 9. As can be seen in the figure, the
360 results by Model 1 and Model 2 are nearly the same, which indicates that considering the shear
361 deformation actually has little influence on the analysis of progressive collapse behavior of precast
362 concrete structures. This conclusion echoes closely observations made in previous researches by
363 (Bao et al. 2008; Yu and Tan 2013; Yu and Tan 2014; Rashidian et al. 2016). Model 3 appears to
364 overestimate the CAA capacity of the specimen, and the bar fracture occurs earlier than the other
365 two models since the fixed-end rotation caused by bar slip at the beam interface is not accounted
366 for in Model 3. On the other hand, Model 1 and Model 4 predict almost the same results, which
367 means developing an equivalent reinforcement model including bond-slip is an alternative way
368 for modeling precast frame sub-assembly under progressive collapse, and the computational
369 efficiency can be also improved.

370 **Effect of concrete strength in cast-in-situ region**

371 Precast concrete structures enables us using concrete of different grades as the cast-in-situ part
372 to improve the integrity of the structure. Therefore, the influence of concrete strength on the
373 progressive collapse resistance is studied. The original concrete strength for the cast-in-situ part in
374 specimen MJ-L-0.88/0.59R is 20.3 MPa, and now cast-in-situ part of 30 MPa and 40 MPa is also
375 simulated. The numerical results are demonstrated in Fig. 10. With the increase of the concrete
376 strength, the CAA capacity will increase; however, the degree of the increase appears to be very
377 limited. Meanwhile, increasing the concrete strength makes little difference to the catenary action,
378 and this is expected since catenary action is mainly controlled by the reinforcement properties. It
379 should be noted that the onset of the bar fracture at the middle column interface becomes earlier
380 with the increase of the concrete strength. This is because the bond strength will rise as the concrete
381 strength increases, resulting in the fracture of bar at a smaller rotation of the beams.

Effect of beam bar properties

The bottom bar directly affect the progressive collapse behavior of the precast assemblages, and it is also closely related to the bond strength in the joint region. Hence the bar diameter and bar strength are studied. The specimen MJ-L-0.88/0.59R is still set as the reference model, in which the bar diameter and yielding strength are 13 mm and 470 MPa, respectively. Then the model is first varied into two new models using different bar diameters, namely 10 mm and 16 mm, respectively, while the bar yield strength remains at 470 MPa. Subsequently, the reference model is varied into another two models using two yielding strengths of 520 MPa and 570 MPa, respectively, while other properties remain unchanged.

The numerical results are shown in Fig. 11 and 12. As can generally be expected, the bar diameter, which in the case herein also represents the amount of reinforcement, has a direct influence on the progressive collapse behavior of the sub-assemblage. The CAA capacity and catenary action capacity both increase with the increase of the bar diameter (and hence amount of reinforcement herein), since the total axial strengths of the beams are controlled by the reinforcing bars. Compared with the reference model, the CAA capacity of the model with a smaller 10-mm bar decreases by 32.1%, while that with a larger 16-mm bar increases by 33.8%. The respective catenary action decreased by 46.8% and increased by 53.4%. Meanwhile, the onset of the transition of the horizontal beam force from compression to tension becomes earlier for model with increased reinforcement, as shown in Fig. 12(b). The concrete will crush earlier for model with larger amount of reinforcement, correspondingly the horizontal force will change to tension earlier.

In a similar trend, with the increase of the bar yielding strength, the CAA capacity and catenary action capacity also exhibit a significant increase, as shown in Fig. 12. With the yield strength increasing from 470 MPa to 520 MPa and 570 MPa, the CAA capacities increase by 8.5% and 16.9%, respectively.

The above results indicates that both the CAA and the catenary capacities tend to increase consistently with the increase of the total strength of the steel reinforcement. Since the total reinforcement strength is closely correlated to the flexural strength of the section, in general design

409 procedure for a precast structure, a certain required degree of progressive collapse resistance may be
410 achieved through controlling the flexure strength of the section, within a reasonable reinforcement
411 ratio range.

412 **Effect of anchorage length at the joint**

413 The anchorage length in the joint region is a crucial point for the precast RC sub-assembly
414 under progressive collapse since it is directly related with the integrity of the joint. Sufficient
415 anchorage length of the bar at the joint will avoid pull-out failure. The original anchorage length
416 for specimen MJ-L-0.88/0.59R is 470 mm. Here variations to 370 mm, 270 mm and 170 mm,
417 respectively, are also simulated. Fig. 13 presents the numerical results for the models with different
418 anchorage lengths. With shorter anchorage length (170 mm and 270 mm), the failure mode of the
419 bar at the middle beam-to-column joint is bar pull-out, while it changes to bar fracture for the cases
420 of anchorage length 370 mm and above. The results for anchorage length 370 mm and 470 mm are
421 basically the same since the anchorage length is sufficient to develop the bond behavior, and thus the
422 generated bond-slip spring property in the Joint2D element are the same. However, for anchorage
423 length 170 mm and 270 mm, pull-out failure will occur prior to fracture according to the derived
424 stress-slip behavior of reinforcement in this paper. Therefore, the failure of the beam interface
425 spring in Joint2D element of this case corresponds to the pull-out failure of the reinforcement bars.
426 However, for all the cases, the ultimate catenary capacities are very close since at this stage the
427 bottom bars all failed (either due to pull-out or due to fracture) and the final catenary capacity is
428 actually determined by the tensile force of the top bars, which is continuous in the models. In
429 general, insufficient anchorage length for the bottom bars will cause pull-out failure at the middle
430 joint, and the beam end flexural capacity will also be reduced due to the failure of the bottom bars.

431 **CONCLUSIONS**

432 In this paper, an efficient numerical model is developed for the progressive collapse analysis
433 of precast RC sub-assemblies. The model is based on the fiber element and Joint2D element in
434 OpenSEES. In particular, to account for the significant bond-slip effect in precast RC structures,
435 the reinforcement stress-slip relationship is analytically derived, and different anchorage types and

436 lengths are considered. To validate the numerical model, a set of recently reported experiments
437 of six precast RC sub-assemblages under a middle column removal scenario are simulated. The
438 results indicate that the proposed model can well capture the typical progressive collapse behaviors
439 of the precast RC structures, including behaviors in the flexural, CAA, and catenary stages.

440 With the validated numerical model, several important factors influencing the analysis of
441 precast structures are investigated, these include the modeling strategy, the post-cast concrete
442 strength, the bar diameter and yielding strength (or total reinforcement contributions), and the
443 bottom bar anchorage length. The results indicate that the bond-slip effect has a sensible influence
444 and therefore should be considered in the numerical model; otherwise the CAA capacity will be
445 overestimated and the beam end rotation capacity will be underestimated. Improving the concrete
446 strength of cast-in-situ part will increase the CAA capacity, but the extent appears to be limited. The
447 reinforcement altogether, through bar diameter and yielding strength, will have a great influence on
448 the CAA capacity as well as the catenary capacity. These two capacities will increase consistently
449 with increasing the bar diameter and yielding strength; but the onset of beam horizontal force
450 transition from compression to tension will also become earlier. The failure mode of the bar at the
451 middle column joint depends on the anchorage length. Pull-out failure will happen for insufficient
452 anchorage length and fracture failure will happen for sufficient anchorage length. However, in both
453 cases the final catenary action capacity is nearly the same in principle since it is dominated by the
454 tensile force of the top bars.

455 In general, the numerical model developed in this paper represents a balanced consideration
456 between the analysis accuracy and computational efficiency. The proposed model approach can be
457 used as an effective tool for progressive collapse analysis of precast structures. It should be noted
458 that some other detailed aspects relating to precast RC structures, like the interface between precast
459 and cast-in-situ concrete surfaces and the bond deterioration, still requires further study in order to
460 be considered in the numerical model.

461 **ACKNOWLEDGEMENTS**

462 The authors would like to acknowledge financial supports from the National Key Research and

463 Development Program of China (No. 2016YFC0701400), the National Natural Science Foun-
464 dation of China (Grant No. 51708106), the Natural Science Foundation of Jiangsu Province
465 (Grant No. BK20170680), and the Fundamental Research Funds for the Central Universities (Nos.
466 2242017k30002, 2242017k40212).

467 APPENDIX I. CONCRETE DAMAGE-PLASTICITY MODEL

468 The uniaxial concrete model used in this paper is based on damage mechanics, and the general
469 form of the constitutive relation can be written as

$$470 \quad \sigma^\pm = (1 - d^\pm) E_c (\epsilon^\pm - \epsilon^{p\pm}) = (1 - d^\pm) E_c \epsilon^{e\pm} \quad (16)$$

471 where σ^\pm is the stress; ϵ^\pm is the total strain; $\epsilon^{p\pm}$ is the plastic strain; d^\pm is the damage variable; E_c
472 is the elastic modulus; the superscript \pm indicate tension and compression, respectively.

473 The damage evolution can be determined by either micro-mechanics (Feng et al. 2016b) or
474 experimental data (Feng et al. 2017), here the latter one is adopted

$$475 \quad d^\pm = \begin{cases} 1 - \frac{\rho^\pm n^\pm}{n^\pm - 1 + (x^\pm)^{n^\pm}} & x^\pm \leq 1 \\ 1 - \frac{\rho^\pm}{\alpha^\pm (x^\pm - 1)^2 + x^\pm} & x^\pm > 1 \end{cases} \quad (17)$$

476 and the symbols are defined as

$$477 \quad x^\pm = \frac{\epsilon^{e\pm}}{\epsilon_c^\pm}, \quad \rho^\pm = \frac{f_c^\pm}{E_c \epsilon_c^\pm}, \quad n^\pm = \frac{E_c \epsilon_c^\pm}{E_c \epsilon_c^\pm - f_c^\pm} \quad (18)$$

478 where f_c^\pm and ϵ_c^\pm are the stress and strain corresponding to the peak strength in tension and
479 compression; E_c is the elastic modulus.

480 The plastic strains are also given by an empirical model, i.e.,

$$481 \quad \begin{cases} \epsilon^{p+} = 0 \\ \epsilon^{p-} = \xi_p (d^-)^{\eta_p} \end{cases} \quad (19)$$

482 where ξ_p and η_p are the plastic parameters that controls the plastic evolution, and the recommended
483 values are 0.6 and 0.1, respectively. Note that the tensile plastic strain is neglected since it is
484 relatively small and has little influence on the overall behavior of concrete.

485 **APPENDIX II. BILINEAR REINFORCEMENT MODEL**

486 The bilinear model is used for reinforcement bars. The stress-strain relation under tension and
487 compression is assumed to be the same, and is given by

$$488 \quad \sigma_s = \begin{cases} E_s \epsilon_s & \epsilon_s \leq \epsilon_y \\ f_y + E_h (\epsilon_s - \epsilon_y) & \epsilon_s > \epsilon_y \end{cases} \quad (20)$$

489 where E_s is the elastic modulus; f_y and ϵ_y are the yielding strength and strain, respectively;
490 $E_h = bE_s$ is the hardening modulus; b is the hardening ratio.

491 **REFERENCES**

- 492 Altoontash, A. (2004). "Simulation and damage models for performance assessment of reinforced
493 concrete beam-column joints." Ph.D. thesis, Stanford University, Stanford University.
- 494 Bao, Y., Kunnath, S. K., El-Tawil, S., and Lew, H. S. (2008). "Macromodel-based simulation of
495 progressive collapse: Rc frame structures." *Journal of Structural Engineering*, 134(7), 1079–
496 1091.
- 497 Bao, Y., Lew, H., and Kunnath, S. K. (2012). "Modeling of reinforced concrete assemblies under
498 column-removal scenario." *Journal of Structural Engineering*, 140(1), 04013026.
- 499 Brunesi, E. and Nascimbene, R. (2014). "Extreme response of reinforced concrete buildings through
500 fiber force-based finite element analysis." *Engineering Structures*, 69, 206–215.
- 501 Brunesi, E., Nascimbene, R., Parisi, F., and Augenti, N. (2015). "Progressive collapse fragility
502 of reinforced concrete framed structures through incremental dynamic analysis." *Engineering*
503 *Structures*, 104, 65–79.
- 504 Brunesi, E. and Parisi, F. (2017). "Progressive collapse fragility models of european reinforced
505 concrete framed buildings based on pushdown analysis." *Engineering Structures*, 152, 579–596.

506 DoD (2013). “Unified facilities criteria: design of buildings to resist progressive collapse.” *Report*
507 *No. UFC 4-023-03*, Department of Defense, Washington DC, United States.

508 Ellingwood, B. R. (2006). “Mitigating risk from abnormal loads and progressive collapse.” *Journal*
509 *of Performance of Constructed Facilities*, 20(4), 315–323.

510 Feng, D.-C., Kolay, C., Ricles, J. M., and Li, J. (2016a). “Collapse simulation of reinforced concrete
511 frame structures.” *The Structural Design of Tall and Special Buildings*, 12(25), 578–601.

512 Feng, D.-C., Ren, X., and Li, J. (2015). “Implicit gradient delocalization method for force-based
513 frame element.” *Journal of Structural Engineering*, 142(2), 04015122.

514 Feng, D.-C., Ren, X., and Li, J. (2016b). “Stochastic damage hysteretic model for concrete based
515 on micromechanical approach.” *International Journal of Non-Linear Mechanics*, 83, 15–25.

516 Feng, D.-C., Wu, G., Sun, Z.-Y., and Xu, J.-G. (2017). “A flexure-shear timoshenko fiber beam
517 element based on softened damage-plasticity model.” *Engineering Structures*, 140, 483–497.

518 GSA (2013). “Alternate path analysis & design guidelines for progressive collapse resistance.”
519 *Report no.*, General Service Administration, Washington DC, United States.

520 Hsu, T. T. (1988). “Softened truss model theory for shear and torsion.” *ACI Structural Journal*,
521 85(6).

522 Kang, S.-B. and Tan, K.-H. (2015a). “Behaviour of precast concrete beam–column sub-assemblages
523 subject to column removal.” *Engineering Structures*, 93, 85–96.

524 Kang, S.-B. and Tan, K.-H. (2015b). “Bond–slip behaviour of deformed reinforcing bars embedded
525 in well-confined concrete.” *Magazine of Concrete Research*, 68(10), 515–529.

526 Kang, S.-B. and Tan, K.-H. (2017). “Progressive collapse resistance of precast concrete frames with
527 discontinuous reinforcement in the joint.” *Journal of Structural Engineering*, 143(9), 04017090.

528 Kang, S.-B., Tan, K.-H., and Yang, E.-H. (2015). “Progressive collapse resistance of precast beam–
529 column sub-assemblages with engineered cementitious composites.” *Engineering Structures*, 98,
530 186–200.

531 Li, Y., Lu, X., Guan, H., and Ren, P. (2016a). “Numerical investigation of progressive collapse
532 resistance of reinforced concrete frames subject to column removals from different stories.”

533 *Advances in Structural Engineering*, 19(2), 314–326.

534 Li, Y., Lu, X., Guan, H., Ren, P., and Qian, L. (2016b). “Probability-based progressive collapse-
535 resistant assessment for reinforced concrete frame structures.” *Advances in Structural Engineer-
536 ing*, 19(11), 1723–1735.

537 Li, Y., Lu, X., Guan, H., and Ye, L. (2011). “An improved tie force method for progressive collapse
538 resistance design of reinforced concrete frame structures.” *Engineering Structures*, 33(10), 2931–
539 2942.

540 Lowes, L. N. and Altoontash, A. (2003). “Modeling reinforced-concrete beam-column joints sub-
541 jected to cyclic loading.” *Journal of Structural Engineering*, 129(12), 1686–1697.

542 Lu, X., Lin, K., Li, Y., Guan, H., Ren, P., and Zhou, Y. (2016). “Experimental investigation
543 of rc beam-slab substructures against progressive collapse subject to an edge-column-removal
544 scenario.” *Engineering Structures*.

545 Mander, J. B., Priestley, M. J., and Park, R. (1988). “Theoretical stress-strain model for confined
546 concrete.” *Journal of Structural Engineering*, 114(8), 1804–1826.

547 Ministry of Construction of the People’s Republic of China, B. (2010). “Code for design of concrete
548 structures.” *Gb50010-2010*, Beijing, China.

549 Pham, A.-T., Tan, K.-H., and Yu, J. (2016). “Numerical investigations on static and dynamic
550 responses of reinforced concrete sub-assemblages under progressive collapse.” *Engineering
551 Structures*.

552 Qian, K. and Li, B. (2011). “Experimental and analytical assessment on rc interior beam-column
553 subassemblages for progressive collapse.” *Journal of Performance of Constructed Facilities*,
554 26(5), 576–589.

555 Qian, K. and Li, B. (2012). “Performance of three-dimensional reinforced concrete beam-column
556 substructures under loss of a corner column scenario.” *Journal of Structural Engineering*, 139(4),
557 584–594.

558 Qian, K., Li, B., and Zhang, Z. (2016). “Influence of multicolumn removal on the behavior of rc
559 floors.” *Journal of Structural Engineering*, 142(5), 04016006.

560 Rashidian, O., Abbasnia, R., Ahmadi, R., and Nav, F. M. (2016). “Progressive collapse of exterior
561 reinforced concrete beam–column sub-assemblages: Considering the effects of a transverse
562 frame.” *International Journal of Concrete Structures and Materials*, 10(4), 479–497.

563 Ren, P., Li, Y., Lu, X., Guan, H., and Zhou, Y. (2016). “Experimental investigation of progressive
564 collapse resistance of one-way reinforced concrete beam–slab substructures under a middle-
565 column-removal scenario.” *Engineering Structures*, 118, 28–40.

566 Sasani, M. and Kropelnicki, J. (2008). “Progressive collapse analysis of an rc structure.” *The
567 Structural Design of Tall and Special Buildings*, 17(4), 757–771.

568 Sasani, M., Werner, A., and Kazemi, A. (2011). “Bar fracture modeling in progressive collapse
569 analysis of reinforced concrete structures.” *Engineering Structures*, 33(2), 401–409.

570 Sezen, H. and Setzler, E. J. (2008). “Reinforcement slip in reinforced concrete columns.” *ACI
571 Structural Journal*, 105(3), 280.

572 Su, Y., Tian, Y., and Song, X. (2009). “Progressive collapse resistance of axially-restrained frame
573 beams.” *ACI Structural Journal*, 106(5), 600.

574 Valipour, H. R. and Foster, S. J. (2010). “Finite element modelling of reinforced concrete framed
575 structures including catenary action.” *Computers & structures*, 88(9), 529–538.

576 Vecchio, F. J. and Collins, M. P. (1986). “The modified compression-field theory for reinforced
577 concrete elements subjected to shear.” *ACI Structural Journal*, ACI, 83(2), 219–231.

578 Yap, S. L. and Li, B. (2011). “Experimental investigation of reinforced concrete exterior beam-
579 column subassemblages for progressive collapse.” *ACI Structural Journal*, 108(5), 542.

580 Yi, W.-J., He, Q.-F., Xiao, Y., and Kunnath, S. K. (2008). “Experimental study on progressive
581 collapse-resistant behavior of reinforced concrete frame structures.” *ACI Structural Journal*,
582 105(4), 433.

583 Yu, J. and Tan, K.-H. (2013). “Experimental and numerical investigation on progressive collapse
584 resistance of reinforced concrete beam column sub-assemblages.” *Engineering Structures*, 55,
585 90–106.

586 Yu, J. and Tan, K.-H. (2014). “Numerical analysis with joint model on rc assemblages subjected to

587 progressive collapse.” *Magazine of Concrete Research*, 66(23), 1201–1218.

588 Yu, X. H., Lu, D. G., Qian, K., and Li, B. (2016). “Uncertainty and sensitivity analysis of reinforced
589 concrete frame structures subjected to column loss.” *Journal of Performance of Constructed
590 Facilities*, 04016069.

591

List of Tables

592

1 Summary of the proposed modeling approach 26

593

2 Reinforcing details of the tested specimens 27

594

3 Material properties of the tested specimens 28

TABLE 1. Summary of the proposed modeling approach

Member	Element	Material	
Beams/columns	DB fiber element	Concrete fibers	ConcreteD
		Steel fibers	Steel01
Beam-to-column connection	Joint2D element	Shear panel	Elastic
		Column interface	Rigid
		Beam interface	Hysteretic

TABLE 2. Reinforcing details of the tested specimens

Specimen	Curtailed bar length (mm)	A-A section		B-B section	
		Top	Bottom	Top	Bottom
MJ-B-0.52/0.35S	900	3H10	2H10	2H10	2H10
MJ-B-0.88/0.59R	1000	3H13	2H13	2H13	2H13
MJ-B-1.19/0.59R	1000	2H16+H13	2H13	2H16+H13	2H13
MJ-L-0.52/0.35S	900	3H10	2H10	2H10	2H10
MJ-L-0.88/0.59R	1000	3H13	2H13	2H13	2H13
MJ-L-1.19/0.59R	1000	2H16+H13	2H13	2H16+H13	2H13

TABLE 3. Material properties of the tested specimens

Bar type	Reinforcement				
	d_b (mm)	f_y (MPa)	f_u (MPa)	E_s (MPa)	ϵ_u (%)
H10	10	462	553	187302	11.9
H13	13	471	568	186526	12.2
H16	16	527	618	196341	11.9
H13*	13	549	698	206600	16.3
H16*	16	573	674	211300	12.9

Specimen	Concrete strength (MPa)	
	Precast units	Cast-in-situ
MJ-B-0.52/0.35S	27.9	35.8
MJ-B-0.88/0.59R	27.9	20.3
MJ-B-1.19/0.59R	40.5	36.1
MJ-L-0.52/0.35S	27.9	35.8
MJ-L-0.88/0.59R	27.9	20.3
MJ-L-1.19/0.59R	27.9	20.3

595	List of Figures	
596	1	Joint2D element for precast sub-assembly under progressive collapse 30
597	2	Determination of the beam end spring property through fiber section analysis . . . 31
598	3	Bond and stress profile of different anchorage types for the precast sub-assembly 32
599	4	Strain profiles of different bar embedded length 33
600	5	Experiments of precast sub-assemblies subjected to progressive collapse by Kang
601		and Tan 34
602	6	Established finite element model 35
603	7	Comparison of numerical and experimental results 37
604	8	Deformed profile for specimen MJ-B-0.88/0.59R 38
605	9	Numerical results for different modeling strategies 39
606	10	Numerical results for cast-in-situ concrete with different strengths 40
607	11	Numerical results for different bar diameters 41
608	12	Numerical results for different bar yielding strengths 42
609	13	Numerical results for different anchorage length 43

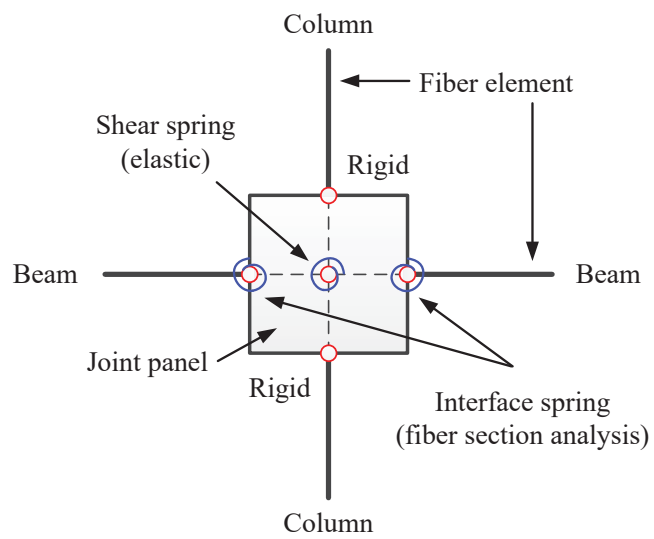


Fig. 1. Joint2D element for precast sub-assembly under progressive collapse

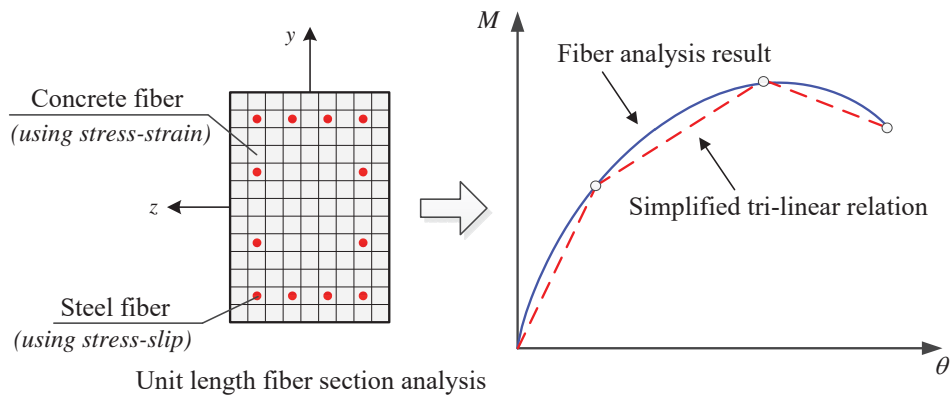
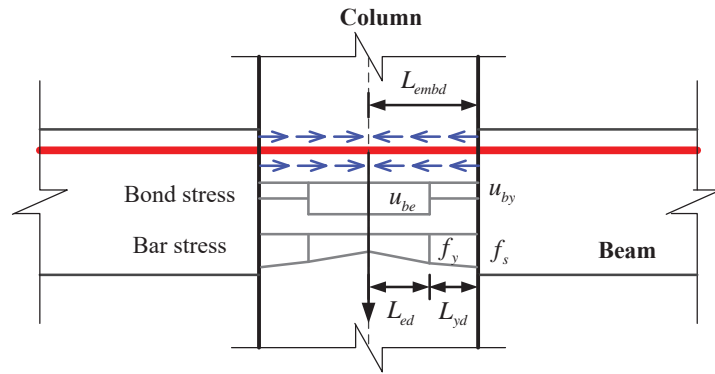
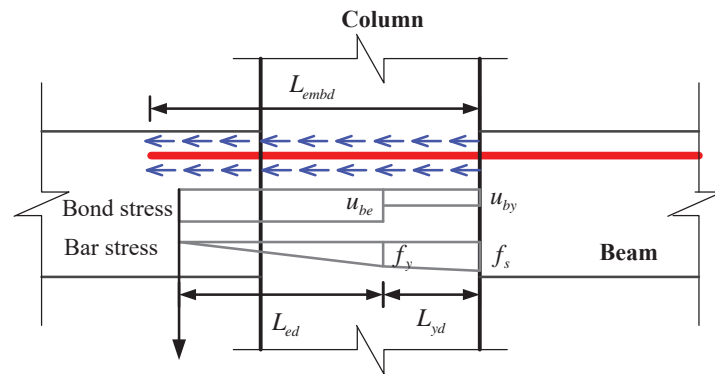


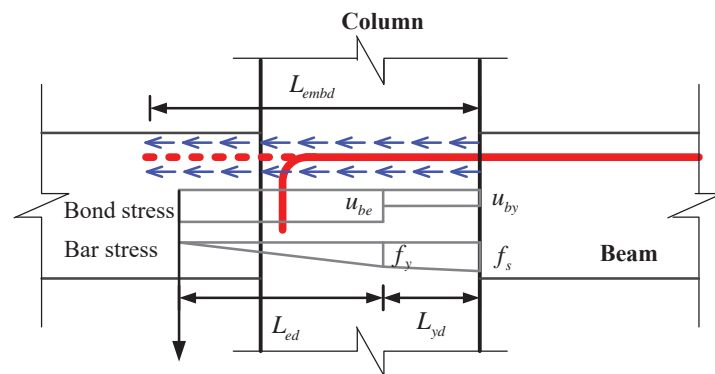
Fig. 2. Determination of the beam end spring property through fiber section analysis



(a) Continuous bar



(b) Lap-spliced bar



(c) Hooked bar

Fig. 3. Bond and stress profile of different anchorage types for the precast sub-assembly

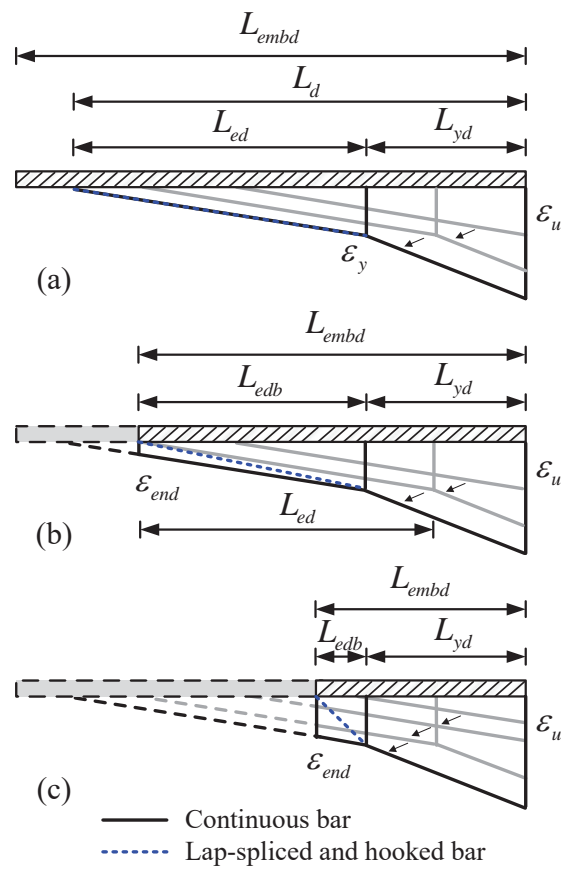
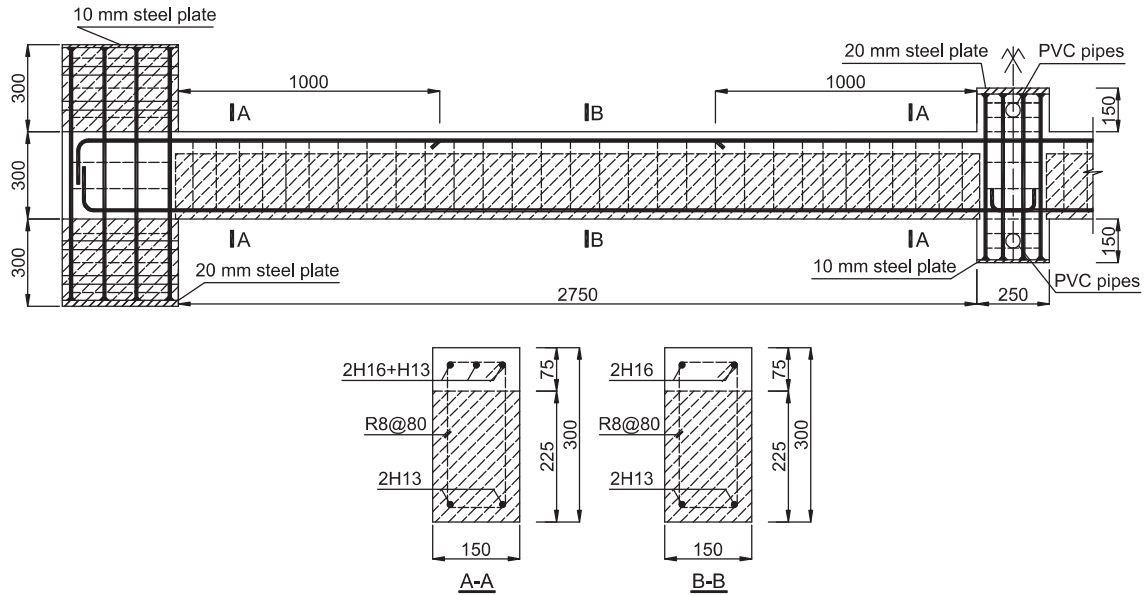
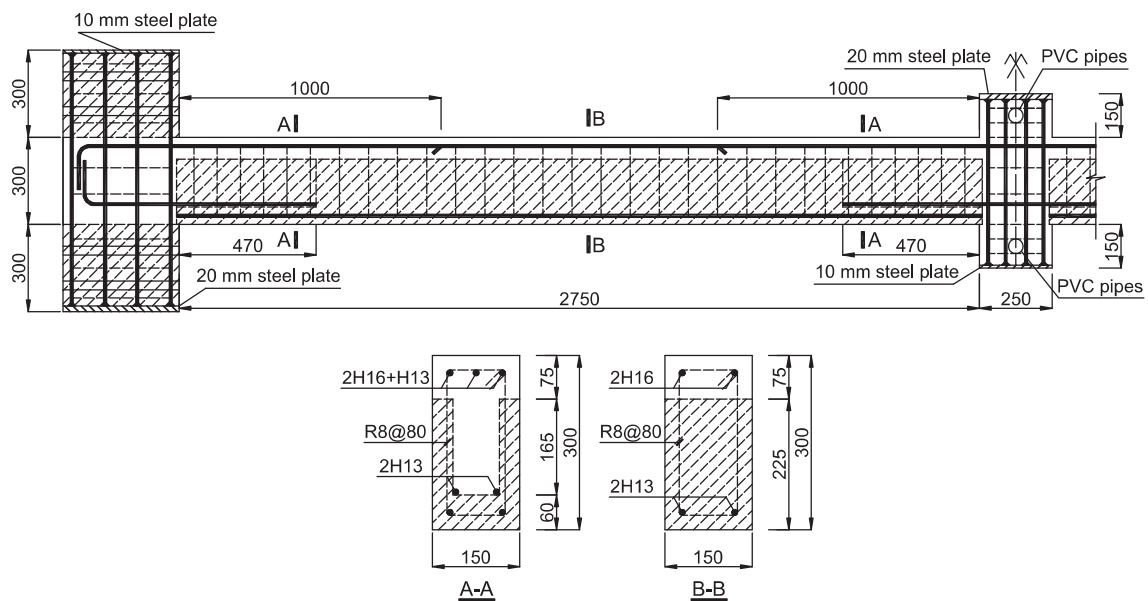


Fig. 4. Strain profiles of different bar embedded length



(a) Hooked bottom reinforcement



(b) Lap-spliced bottom reinforcement

Fig. 5. Experiments of precast sub-assemblages subjected to progressive collapse by Kang and Tan

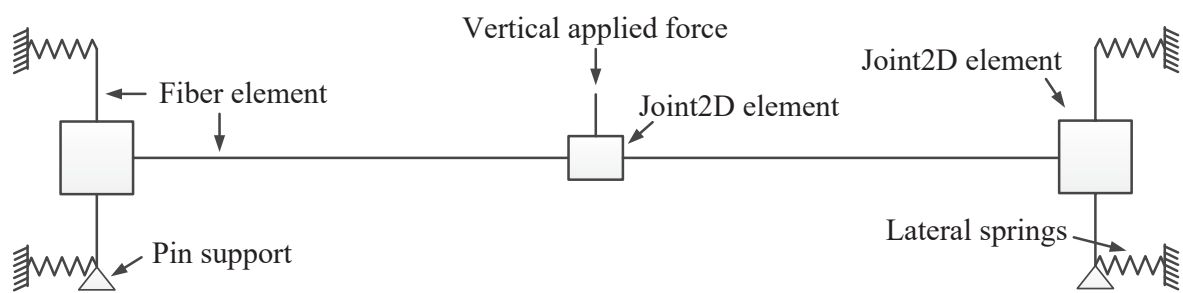
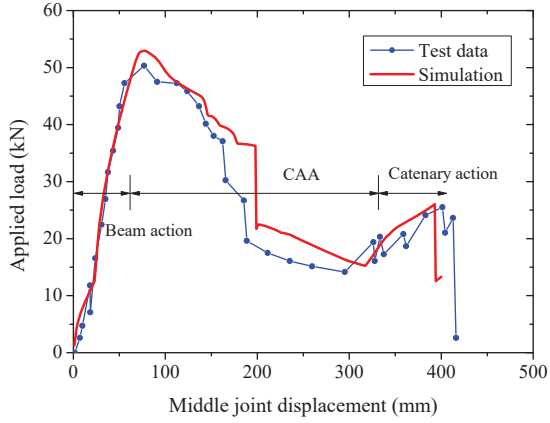
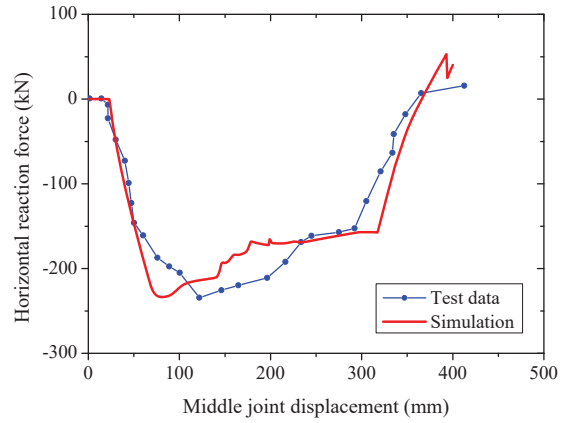


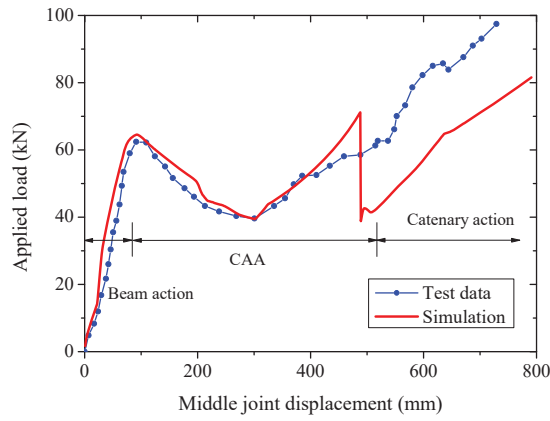
Fig. 6. Established finite element model



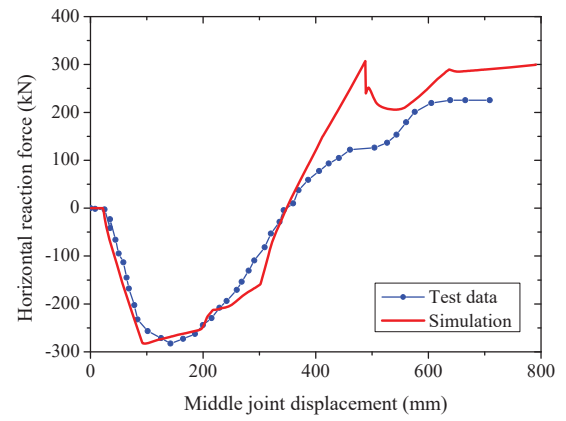
(a) MJ-B-0.52/0.35S-vertical



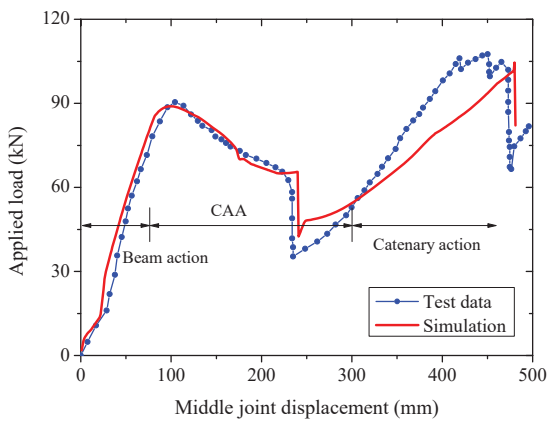
(b) MJ-B-0.52/0.35S-horizontal



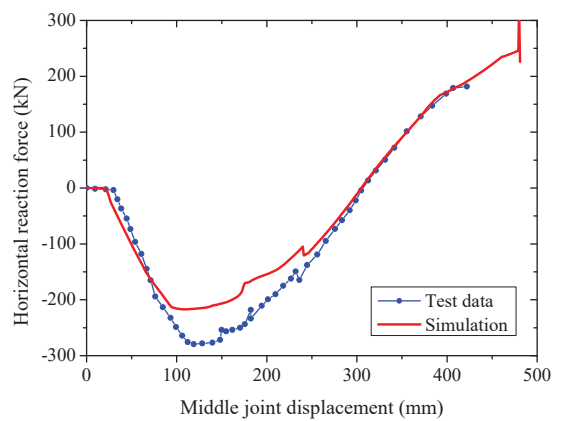
(c) MJ-B-0.88/0.59R-vertical



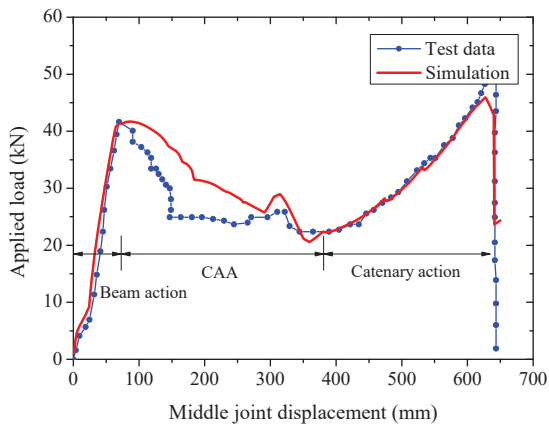
(d) MJ-B-0.88/0.59R-horizontal



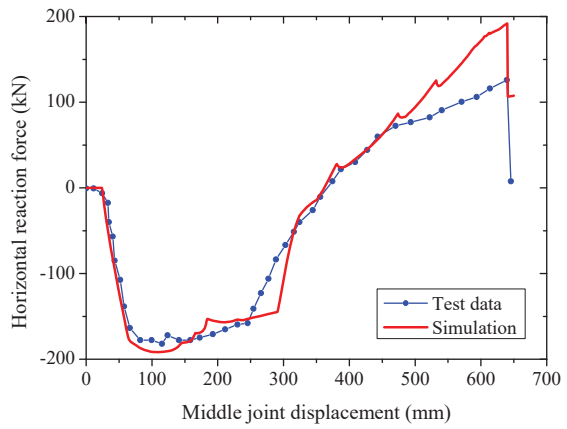
(e) MJ-B-1.19/0.59R-vertical



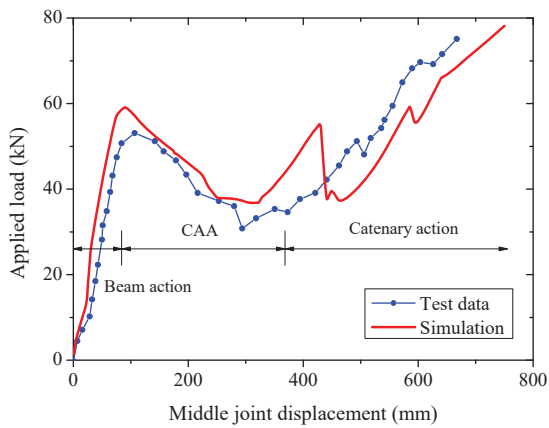
(f) MJ-B-1.19/0.59R-horizontal



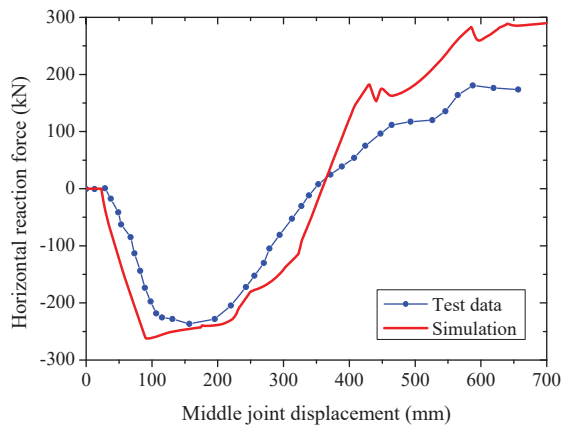
(g) MJ-L-0.52/0.35S-vertical



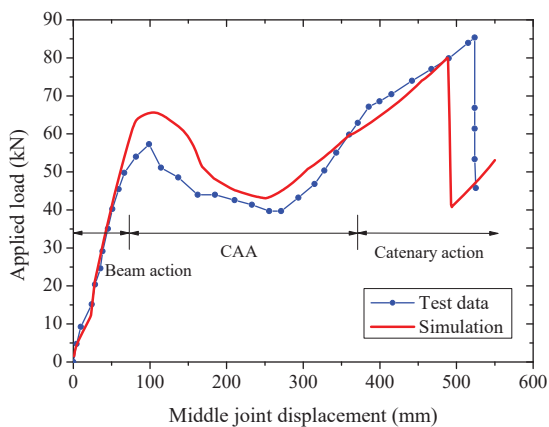
(h) MJ-L-0.52/0.35S-horizontal



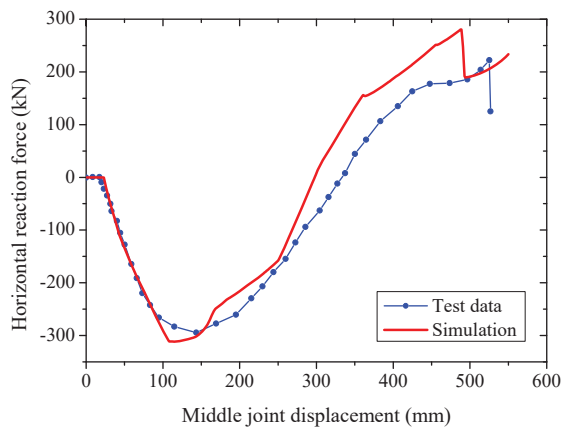
(i) MJ-L-0.88/0.59R-vertical



(j) MJ-L-0.88/0.59R-horizontal



(k) MJ-L-1.19/0.59R-vertical



(l) MJ-L-1.19/0.59R-horizontal

Fig. 7. Comparison of numerical and experimental results

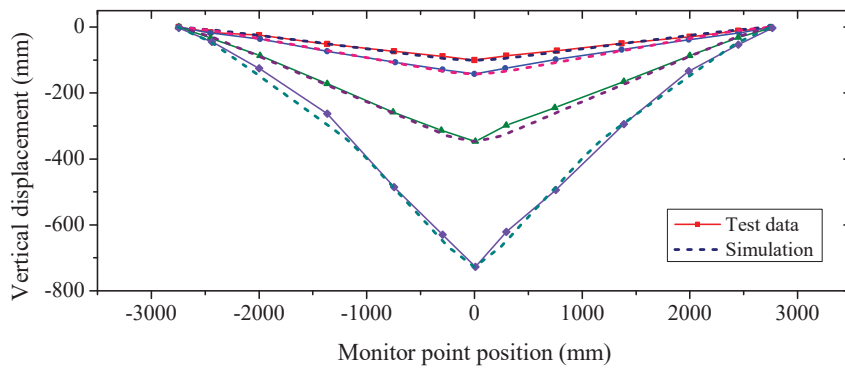


Fig. 8. Deformed profile for specimen MJ-B-0.88/0.59R

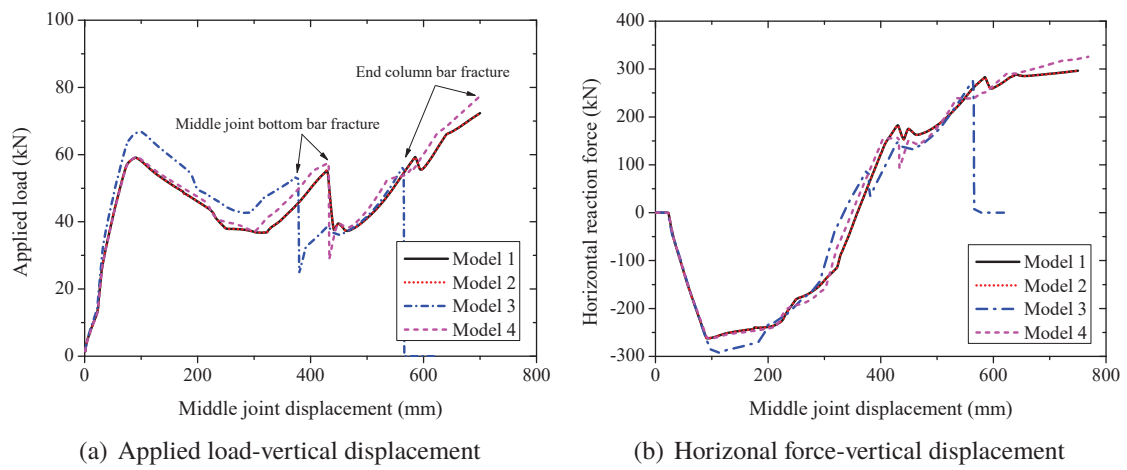


Fig. 9. Numerical results for different modeling strategies

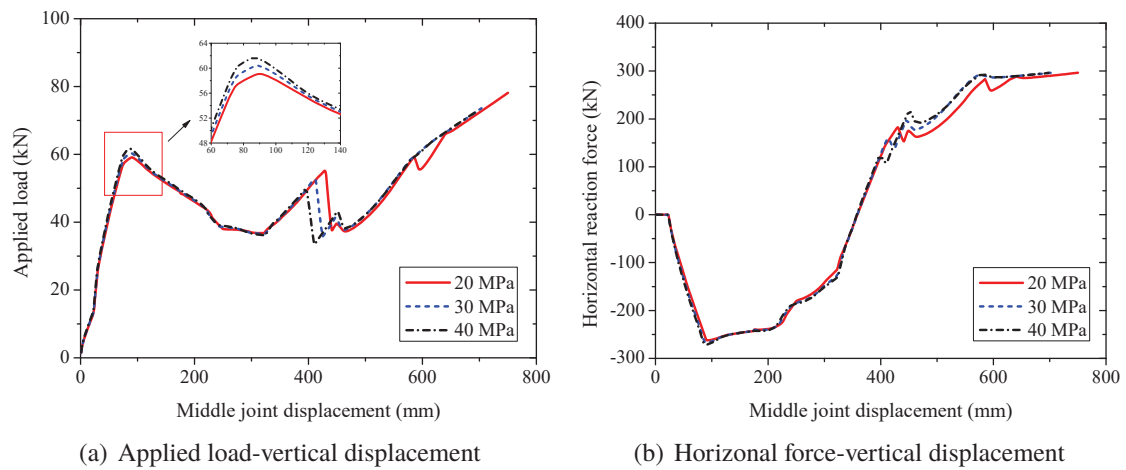
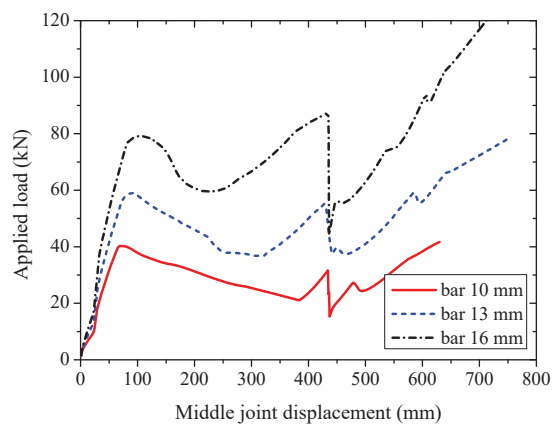
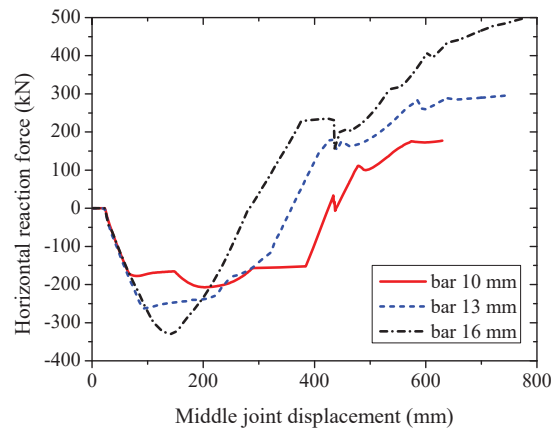


Fig. 10. Numerical results for cast-in-situ concrete with different strengths

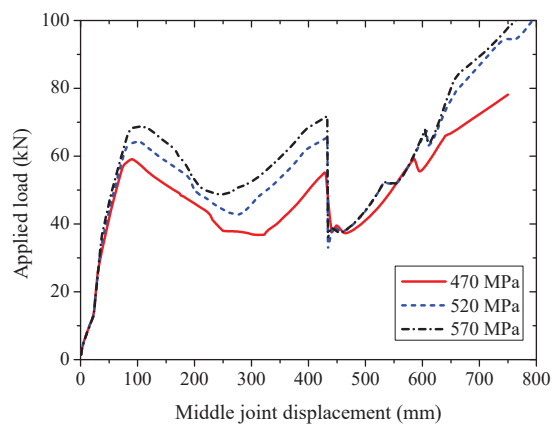


(a) Applied load-vertical displacement

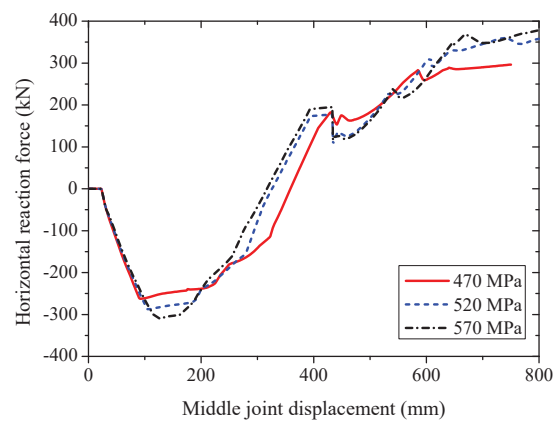


(b) Horizontal force-vertical displacement

Fig. 11. Numerical results for different bar diameters



(a) Applied load-vertical displacement



(b) Horizontal force-vertical displacement

Fig. 12. Numerical results for different bar yielding strengths

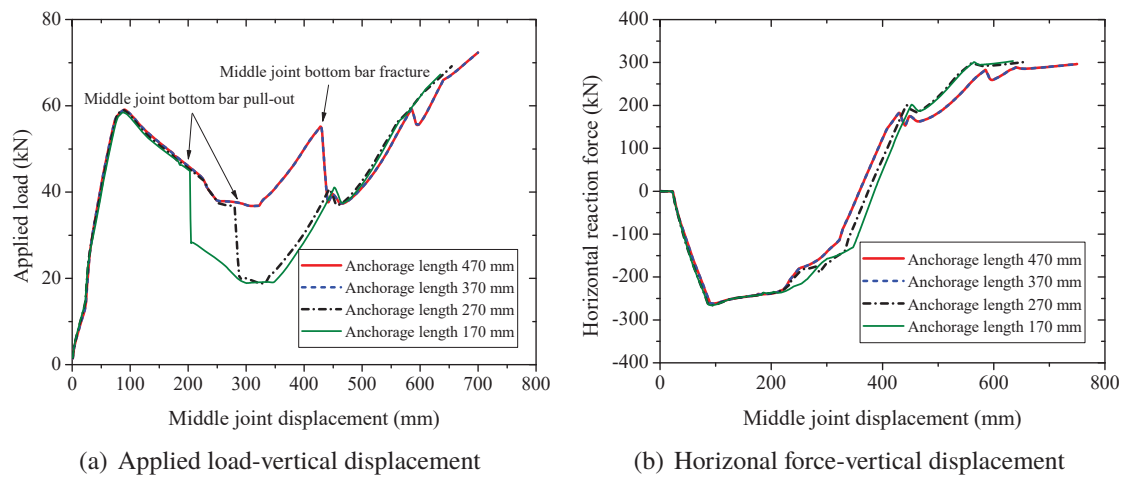


Fig. 13. Numerical results for different anchorage length